Quasiperiodic Krönig-Penney model on a Fibonacci superlattice

Autor(en): **Würtz, D. / Soerensen, M.P. / Schneider, T.**

Objekttyp: **Article**

Zeitschrift: **Helvetica Physica Acta**

Band (Jahr): **61 (1988)**

Heft 3

PDF erstellt am: **23.05.2024**

Persistenter Link: https://doi.org/10.5169/seals-115936

Helvetica Physica Acta, Vol. **61** (1988) 345–362

0018–0238/88/030345–18$1.50 + 0.20/0

Quasiperiodic Krönig–Penney model on a Fibonacci superlattice

By D. Würtz,[1]) M. P. Soerensen[2]) and T. Schneider

IBM Research, Zurich Research Laboratory, CH-8803 Rüschlikon, Switzerland

(23. X. 1987)

Abstract. We study the propagation of electrons in a one-dimensional Krönig–Penney model on a Fibonacci superlattice. We consider two different models, one with δ-function potentials and the other with finite potential barriers. The nature of the eigenstates, the integrated density of states and inverse localization length, as well as transmission and reflectance are investigated. In contrast to periodic arrangements, we observe a self-similar structure in the wavenumber or energy dependence of the physical quantities exhibiting scaling properties and multifractal behavior.

1. Introduction

The problem of electron propagation through a one-dimensional array of potential barriers has attracted considerable interest since its introduction more than half a century ago by Krönig and Penney [1] for a periodic chain. In the last two decades, much effort has been devoted to the study of static and transport properties of electrons in disordered systems. Recognition of the importance of localization has led to many calculations [2] of inverse exponential localization length, integrated density of states and resistance, leading to a well-understood scaling theory [3]. Recently, quasiperiodic systems attracted wide attention [4] as structures being intermediate between truly disordered and periodic ones. Unlike for random or ordered chains, for which the states are exponentially localized or extended, quasiperiodic or incommensurate systems exhibit novel features: Metal-insulator transition for a critical potential strength [5], self-similar, fractal and multifractal behavior [6], algebraic localization of wavefunctions [7]. Another interesting feature is the connection to dynamic maps. In fact, transforming the Schrödinger problem to a tight-binding model, transfer matrix techniques and renormalization-group concepts can be applied and provide the connection to nonlinear maps. Energies belonging to the spectrum, scaling properties of the integrated density of states, wavefunctions and transmission coefficient then follow from the properties of these maps.

---

[1]) Permanent address: Institut für Theoretische Physik, Universität Heidelberg, Philosophenweg 19, D-6900 Heidelberg, FRG.

[2]) Permanent address: Laboratory of Applied Mathematical Physics, Technical University of Denmark, Building 303, DK-2800 Lyngby, Denmark.

In this work, we concentrate on quasiperiodic potentials constructed from two different barriers A and B built together according to the Fibonacci inflation rule. Such structures can be manufactured by means of the molecular-beam epitaxy technique [8]. Previously, the tight-binding and δ-function potential versions of the associated Schrödinger problem attracted particular attention. Here we consider, in view of experimental realizations, the more realistic case of rectangular potential barriers.

In Section 2, we study the δ-potential version of the Krönig–Penney model, and sketch the basic formalism to calculate properties of interest. Here, we treat the limit of vanishing barrier width and diverging barrier height with constant potential strength. Strength and/or spacing of the δ potentials are arranged according to the Fibonacci sequence. The Schrödinger equation for this problem is then transformed to a Poincaré map, corresponding to a difference equation of a modified tight-binding model. This is achieved by rewriting the complex first-order transfer-matrix recursion relation as a real second-order scalar relation from which the eigenvalue spectrum is obtained by node counting. Using the transfer-matrix formalism and the Poincaré map, we also evaluate the exponential growth rate of wavefunctions and the transmission coefficient. At sufficiently low energies, the numberical results reveal a highly fragmented integrated density of states, becoming smoother with increasing energy. The occurrence of *band-like* behavior in the high-energy domain differs essentially from the tight-binding model. Nevertheless, in analogy to this model we find scaling properties, which are traced back to cycles in the trace map of the transfer matrices.

In Section 3, we turn to the more realistic case of rectangular barriers to investigate the modifications introduced by the finite-barrier width and height. Here, we concentrate on systems of finite length. In the domain of narrow barriers, integrated density of states and transmission agree fairly well with the δ-function model, with potential strength equal to the area of the rectangular barrier. For broader barriers with a width becoming comparable with the lattice spacing, quantitative differences appear. Nevertheless, the highly fragmented structure of the integrated density of states and the self-similar behavior of the transmission are still maintained and are in qualitative agreement with the δ-function potential model. In Section 4, we discuss and summarize our main results.

2. δ-function model

We first consider the one-dimensional time-independent Schrödinger equation

$$-\frac{\hbar^2}{2m}\frac{\partial^2\psi(x)}{\partial x^2}+\sum_{n=1}^{N} W_n\delta(x-x_n)\psi(x)=E\psi(x) \tag{1}$$

with a Krönig–Penney potential consisting of an array of δ functions with

strength W_n at positions x_n. In the following, we consider dimensionless quantities and measure all energies in units of $\hbar^2/2m(\Delta L)^2$ and all lengths in units of a mean lattice spacing $\Delta L = L/N$, where L is the total length of the system and N the total number of lattice cells. Note that the potential W_n has units of energy/length since the δ-functions $\delta(x - x_n)$ have dimension 1/length. Both potential strengths W_n and distances between the δ-functions $\Delta_n = x_n - x_{n-1}$ may have either of two different values $(W_n, \Delta_n) = (W_A, \Delta_A)$ or (W_B, Δ_B), according to the Fibonacci sequence. This sequence follows from the inflation rule: $S_1 = A$, $S_2 = AB$, $S_3 = ABA$, $S_4 = ABAAB, \ldots, S_{l+1} = S_l S_{l-1}$. Letters A and B label the elements with potential strength and intersite distance (W_A, Δ_A) and (W_B, Δ_B), respectively. The number of elements is given by the Fibonacci numbers $F_{l+1} = F_{l-1} + F_l$ with initial conditions $F_0 = F_1 = 1$. Alternatively, the sequence can be obtained from the rule

$$\lambda_{n+1} = [\theta_n + 1/\sigma_G], \qquad \theta_{n+1} = (\theta_n + 1/\sigma_G) : \mathrm{mod}\ 1, \tag{2}$$

which is more convenient for numerical applications. The rectangular bracket $[\ldots]$ denotes the integer part, and $\sigma_G = \lim_{l\to\infty}(F_{l+1}/F_l) = (\sqrt{5}+1)/2$ is the golden mean. The Fibonacci sequence is then obtained by adding element A at lattice site $x_n = x_{n-1} + \Delta_A$ if λ_n equals 1, and element B at position $x_n = x_{n-1} + \Delta_B$ if λ_n equals 0, starting at $n = 1$ with $\theta_0 = 0$.

For $\Delta_n = \Delta$ and $W_n = W$, the Schrödinger equation (1) corresponds to the periodic $\delta - f$ Krönig–Penney model [1], which has been studied for half a century and is well documented in textbooks [9] on solid-state physics. For random potential strength, one obtains a model for random alloys. This model also has a long history, starting with the pioneering work of Schmidt [10]. Subsequently, it was treated analytically and numerically by many authors. If only the distances Δ_n are randomly distributed it will describe electrons in a one-dimensional liquid. In the more general situation, where Δ_n and W_n are random, the Schrödinger equation can be interpreted as a model for a liquid alloy. Some examples for special kinds of disorder were discussed by Niewenhuizen [11]. For a review and further references, we refer to [11] and to the article of Erdös and Herndon [12]. In the intermediate quasiperiodic case, two different situations can also be distinguished. *Model I:* Equally-spaced binary potentials arranged according to the Fibonacci sequence. *Model II:* Identical potentials with intersite distances given by the Fibonacci sequence. Some properties of this model have been studied by Kollar and Süto [13], and Hu and Ting [14].

To evaluate the energy spectrum and the transmission properties, it is convenient to use the transfer-matrix technique. The transfer matrix, relating the wavefunctions of adjacent cells, is obtained for a system of N sites as the product of the individual transfer matrices for each cell. Next, we sketch the derivation of this formalism for the Fibonacci model. Let us consider the interval $x \in [x_n, x_{n+1}]$, where the solution of the Schrödinger equation (1) can be written as

$$\psi_n(x) = A_n e^{ik(x-x_n)} + B_n e^{-ik(x-x_n)}. \tag{3}$$

$k = \sqrt{E}$ denotes the wavenumber. Next, we match the wavefunctions on the right and left of a δ-function potential, by imposing continuity of the wavefunction and discontinuity of its slope. This yields the transfer matrix $\mathbf{P}^n$, relating the amplitudes (A_n, B_n) and (A_{n-1}, B_{n-1}) for the transfer of an electron from one cell to the next:

$$\begin{pmatrix} A_n \\ B_n \end{pmatrix} = \mathbf{P}^n \begin{pmatrix} A_{n-1} \\ B_{n-1} \end{pmatrix} = \begin{pmatrix} P_{11}^n & P_{12}^n \\ P_{21}^n & P_{22}^n \end{pmatrix} \begin{pmatrix} A_{n-1} \\ B_{n-1} \end{pmatrix}. \tag{4}$$

The elements P_{ij}^n of the unimodular transfer matrix $\mathbf{P}^n$ are given by

$$\begin{aligned} P_{11}^n &= \left(1 - i\frac{W_n}{2k}\right) \exp(ik\Delta_n), & P_{12}^n &= -i\frac{W_n}{2k} \exp(-ik\Delta_n), \\ P_{21}^n &= i\frac{W_n}{2k} \exp(ik\Delta_n), & P_{22}^n &= \left(1 + i\frac{W_n}{2k}\right) \exp(-ik\Delta_n), \end{aligned} \tag{5}$$

and the total transfer matrix $\mathbf{P}_N$ for a lattice with N cells is obtained from

$$\mathbf{P}_N = \prod_{i=N}^{1} \mathbf{P}^i. \tag{6}$$

For finite chains, the eigenvalue spectrum and the transmission properties are then obtained as follows: Let the lattice start at $x = x_0 = 0$ and end at $x = x_N = L$. Imposing periodic boundary conditions $\psi_0(x = 0) = \psi_N(x = L)$ and $\psi_0'(x = 0) = \psi_N'(x = L)$, the total transfer matrix $\mathbf{P}_N$ must satisfy

$$(A_N, B_N) = \mathbf{P}_N(A_0, B_0) = (A_0, B_0). \tag{7}$$

This equation possesses a non-zero solution for (A_0, B_0) only, when the determinant $\det(\mathbf{P}_N - \mathbf{I}) = 0$, where $\mathbf{I}$ is the identity matrix. Using the facts that $\det(\mathbf{P}_N) = 1$ and $\det(\mathbf{P}_N - \mathbf{I}) = 0$, yields the following relation for the trace of $\mathbf{P}_N$:

$$\tfrac{1}{2} \operatorname{Tr} \mathbf{P}_N = \tfrac{1}{2}(P_N^{11} + P_N^{22}) = 1. \tag{8}$$

Accordingly, energies satisfying this condition are eigenvalues. Similarly, eigenvalues corresponding to antiperiodic boundary conditions, $A_N = -A_0$, $B_N = -B_0$, can be obtained from $\frac{1}{2} \operatorname{Tr} \mathbf{P}_N = -1$. The transmission coefficient τ_N and the reflection coefficient ρ_N are defined by

$$\tau_N = \frac{|A_N|^2}{|A_0|^2} = \frac{1}{|P_N^{11}|^2}, \qquad \rho_N = \frac{|B_0|^2}{|A_0|^2} = \frac{|P_N^{21}|^2}{|P_N^{22}|^2}, \tag{9}$$

τ_N being the probability that an incident particle is transmitted through the lattice of size N, and ρ_N the probability that the particle is reflected. It can easily be verified that conservation of probability leads to the relation $\tau_N + \rho_N = 1$.

Next, we sketch a completely different approach to evaluate the properties of interest. The goal is to transform the complex matrix recursion relation (4) to a real scalar difference equation. Here, we adopt ideas of a French group [15] and

transform the amplitudes (A_n, B_n) into (ϕ_{n+1}, ϕ_n):

$$\begin{pmatrix} \phi_{n+1} \\ \phi_n \end{pmatrix} = \begin{pmatrix} e^{ik\Delta_{n+1}} & e^{-ik\Delta_{n+1}} \\ 1 & 1 \end{pmatrix} \begin{pmatrix} A_n \\ B_n \end{pmatrix} = \mathbf{T}^{n+1} \begin{pmatrix} A_n \\ B_n \end{pmatrix}, \tag{10}$$

where $\phi_n \equiv \psi_n(x_n)$. In analogy to equation (4), we then obtain a recursion relation for (ϕ_{n+1}, ϕ_n), namely,

$$\begin{pmatrix} \phi_{n+1} \\ \phi_n \end{pmatrix} = \tilde{\mathbf{P}}^{n,n+1} \begin{pmatrix} \phi_n \\ \phi_{n-1} \end{pmatrix} = \begin{pmatrix} \tilde{P}_{11}^{n,n+1} & \tilde{P}_{12}^{n,n+1} \\ 1 & 0 \end{pmatrix} \begin{pmatrix} \phi_n \\ \phi_{n-1} \end{pmatrix}. \tag{11}$$

The transfer matrix $\tilde{P}^{n,n+1}$ is given by

$$\begin{aligned} \tilde{P}_{11}^{n,n+1} &= \frac{\sin(k\Delta_n + k\Delta_{n+1})}{\sin(k\Delta_n)} + \frac{W_n}{k} \sin(k\Delta_{n+1}), \\ \tilde{P}_{12}^{n,n+1} &= -\frac{\sin(k\Delta_{n+1})}{\sin(k\Delta_n)}. \end{aligned} \tag{12}$$

This form is very useful for numerical applications, since the recursion relation leads to a scalar difference equation

$$\phi_{n+1} = \tilde{P}_{11}^{n,n+1} \phi_n + \tilde{P}_{12}^{n,n+1} \phi_{n-1}. \tag{13}$$

For *Model I*, where $\Delta_n = \Delta_{n+1} = \Delta$, this formula is further simplified to

$$\phi_{n+1} + \phi_{n-1} = \left\{ 2\cos(k\Delta) + \frac{W_n}{k} \sin(k\Delta) \right\} \phi_n. \tag{14}$$

This equation is formally identical to a tight-binding model $\phi_{n+1} + \phi_{n-1} = (\omega + V_n)\phi_n$ with energy $\omega = 2\cos(k\Delta)$, and potential $V_n = W_n \sin(k\Delta)/k$. For this model, it has been verified [15] that equations (1) and (14) yield identical results for infinite chains. Thus, the characteristic function yielding the integrated density of states by node counting, and the inverse localization length [16] can now be evaluated in terms of a scalar recursion relation. Moreover, the characterization and classification of the states can be obtained from a simple recursion relation for the trace of the associated transfer matrix on the Fibonacci sublattice F_l. Evaluation of the transfer matrix is not required. On this sublattice, the total transfer matrix is given by $\mathbf{P}_{l+1} = \mathbf{P}_{l-1}\mathbf{P}_l$. Its trace, $x_l = \frac{1}{2} \operatorname{Tr} \mathbf{P}_l$ satisfies the recursion relation [7]

$$x_{l+1} = 2x_l x_{l-1} - x_{l-2}, \tag{15}$$

with initial conditions, depending on wavenumber k or energy E:

$$\begin{aligned} x_{-1} &= \cos(k\Delta_A - k\Delta_B) + \frac{W_A - W_B}{2k} \sin(k\Delta_A - k\Delta_B), \\ x_0 &= \cos(k\Delta_B) + \frac{W_B}{2k} \sin(k\Delta_B), \\ x_1 &= \cos(k\Delta_A) + \frac{W_A}{2k} \sin(k\Delta_A). \end{aligned} \tag{16}$$

Equations (12), (14) and (16) are valid for positive energies E. For negative energies, the cosine and the sine have to be replaced by cosh- and sinh-functions, respectively. It is well-known and easy to check that the iteration of the trace map x_l has the l-independent invariant,

$$I = x_{l+1}^2 + x_l^2 + x_{l-1}^2 - 2x_{l+1}x_l x_{l-1} - 1. \tag{17}$$

I can be evaluated from the initial conditions for the trace map (16) by setting $l = 0$. The resulting expressions are rather ugly, but simplify for *Model I* and *Model II* to

$$\begin{aligned} I_{\text{Model I}} &= \left\{ \tfrac{1}{2} W \frac{\sin(k\Delta_A - k\Delta_B)}{k} \right\}^2, \\ I_{\text{Model II}} &= \left\{ \tfrac{1}{2} (W_A - W_B) \frac{\sin(k\Delta)}{k} \right\}^2. \end{aligned} \tag{18}$$

In contrast to the usual tight-binding model [7, 17] invariant I depends in the present case on the wavenumber k. Hence, iterations evolve for different energies on different surfaces.

From the tight-binding model, it is well-known that for energies in the spectrum the iterates x_l (cyclic or aperiodic) remain bounded. If x_l escapes to infinity with increasing l, we shall have a gap state [7]. This fact and the observation that the nonlinear trace map yields a strange repeller imply a highly fragmented Cantor-type spectrum. This expectation is fully confirmed by numerical results for the integrated density of states $N(E)$ and the inverse localization length $\gamma(E)$ shown in Fig. 1. Here, we assumed the potential strengths

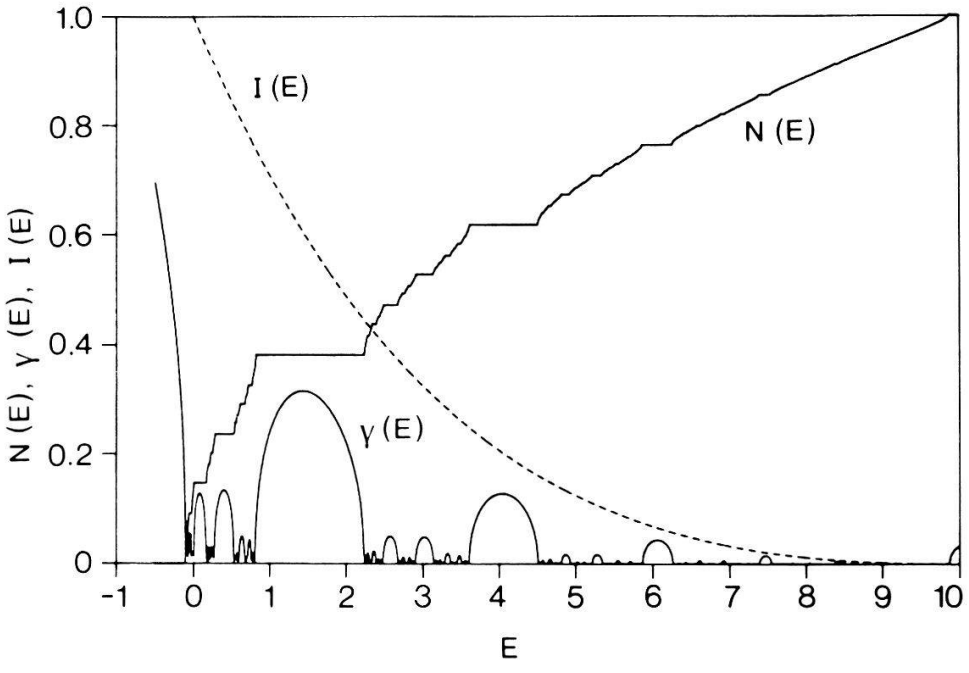

Figure 1
Integrated density of states $N(E)$, inverse exponential growth-rate $\gamma(E)$ and invariant $I(E)$ versus energy E for the δ-function Krönig–Penny model with parameters $V_A = -V_B = 1$ and $\Delta_A = \Delta_B = 1$ for a chain of length $N \sim 10^6$.

$W_A = -W_B = 1$. The spectrum can be classified as follows:

i) Energies within a *gap* which do not belong to the spectrum. The amplitudes of the wavefunctions grow exponentially with length n. Thus, the iterates of the trace map escape.

ii) Energy values lying on a *gap edge*, either top or bottom, where the trace map exhibits a six-cycle or 12-cycle, depending on the parameters of the model. For the ground state, we observe a two-cycle.

iii) *Internal-energy* values surrounded in both directions by other energies belonging to the spectrum. A typical trajectory of the trace map x_l is aperiodic, although periodic ones are also possible.

iv) *Band-like behavior* is found in the upper energy part of the spectrum. In this energy region, a generic-energy value leads to a *chaotic* trajectory of x_l. It is numerically stable over many thousands of iterations. In this energy region, transmission is almost perfect.

Some of these features are apparent from Fig. 1, showing the integrated density of states. The invariant $I(E)$ is also depicted, measuring the degree of fragmentation. With increasing energy E, invariant $I(E)$ becomes smaller and vanishes at $E = \pi^2$. Similarly, the length of the main gaps in $N(E)$ and the main peak heights in $\gamma(E)$ are seen to decrease with increasing E. We now turn to some special energies in the spectrum.

The bottom or *ground state* of the spectrum exhibits a two-cycle (a, b) in the trace map (15). The values of a and b can be evaluated from the invariant (17) and the trace map (15),

$$\begin{aligned} I &= a^2 + b^2 - ab - 1, \\ a + b &= 2ab. \end{aligned} \tag{19}$$

Solving the second equation for b, and inserting it in the first equation for the invariant I we obtain the following quartic equation:

$$z^4 - \tfrac{3}{2}z^3 - \tfrac{1}{4}(1 + 4I)z^2 + (1 + I)z - \tfrac{1}{4}(1 + I) = 0, \tag{20}$$

where we have replaced the variable a by z. Since the numerical value for a is *a priori* a solution of this equation, $b = a/(2a - 1)$ is also one. The remaining two solutions are denoted by $\bar{a}$ and $\bar{b}$. Thus, the quartic equation can be written as $(z - a)(z - b)(z - \bar{a})(z - \bar{b}) = 0$. Performing the multiplications and comparing the coefficients, we finally obtain

$$\begin{aligned} a &= \gamma_+ + \sqrt{\gamma_+(\gamma_+ - 1)}, \qquad & b &= \gamma_+ - \sqrt{\gamma_+(\gamma_+ - 1)}, \\ \bar{a} &= \gamma_- + \sqrt{\gamma_-(\gamma_- - 1)}, \qquad & \bar{b} &= \gamma_- - \sqrt{\gamma_-(\gamma_- - 1)}. \end{aligned} \tag{21}$$

$\gamma_\pm$ depends on the invariant I, and is given by

$$\gamma_\pm = \tfrac{1}{8}(3 \pm \sqrt{25 + 16I}). \tag{22}$$

Besides cycle (a, b), $(\bar{a}, \bar{b})$ also yields a two-cycle. This is easily verified by noting that both pairs of solutions (a, b) and $(\bar{a}, \bar{b})$ satisfy the invariant and trace map simultaneously. Linearization of map (15) around the above-mentioned two-cycle

leads to three eigenvalues, one equaling unity and the other two given by $\lambda^{(\pm)}$ and $1/\lambda^{(\pm)}$, where

$$\lambda^{(\pm)} = \alpha^{(\pm)} \pm \sqrt{(\alpha^{(\pm)})^2 - 1}, \qquad \alpha^{(\pm)} = \tfrac{1}{2}(1 - 8\gamma_{\pm}). \tag{23}$$

Subscript $(\pm)$ on $\alpha^{(\pm)}$ means that the (+) solution belongs to cycle (a, b), and the (-) solution to cycle $(\bar{a}, \bar{b})$, respectively. This fixed-point analysis implies scaling. Following [6] and [17], scaling predicts for the integrated density of states $N(E^* + \Delta E)$ and energies around E^* leading to the two-cycle,

$$|N(E^* + \Delta E) - N(E^*)| \sim (\Delta E)^{\bar{x}} G\left(\frac{X}{S} \ln |\Delta E|\right) \tag{24}$$

with scaling exponent

$$\bar{x} = \frac{2 \ln \sigma_G}{|\ln|\lambda||}. \tag{25}$$

The amplitude is periodic with period $S/\bar{X}$, where S is the vertical spacing of the major gaps on a logarithmic scale. In the present case, $S = 2 \ln(\sigma_g)$, yielding the period $\Delta p = \ln |\lambda|_{\max}$. Numerical results depicting these scaling features are shown in Fig. 2. For potential strengths $W_A = -W_B = 1$ and uniform lattice spacing, our estimate for the ground-state energy is $E^* = E_{\text{bot}} = -0.10373014133295410132683, \ldots$, yielding $I(E^*) = 1.035 \cdots$. From equations (21) and (22), the amplitudes of the two-cycle are $(a, b) = (1.643, \ldots, 0.7187 \cdots)$ as numerically verified over approximately 50 iterations, (Fig. 3a). Invoking then equation (23), the eigenvalue λ can be evaluated,

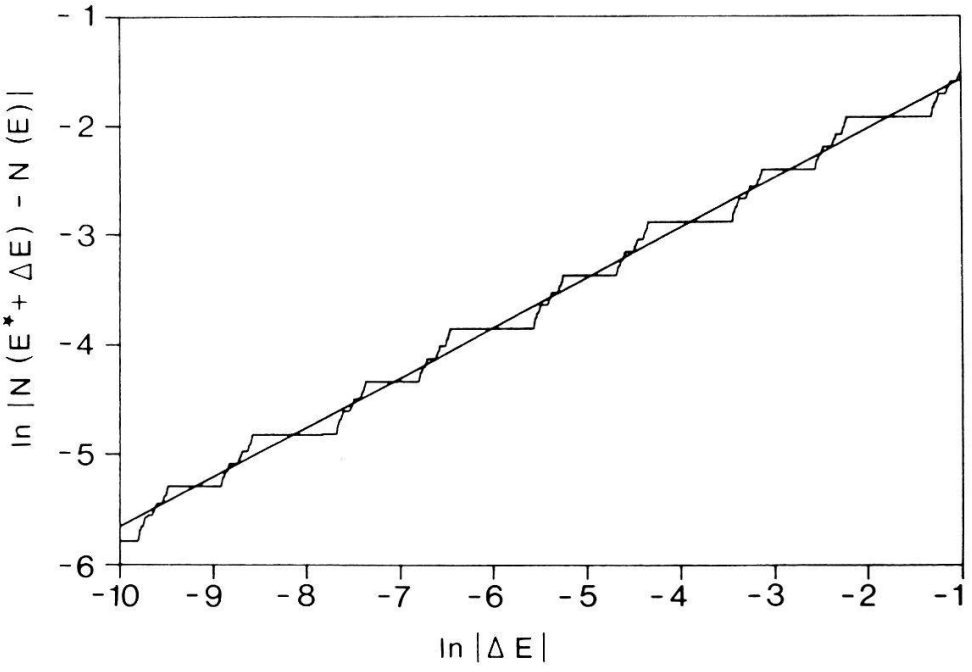

Figure 2
Scaling behavior $\ln |N(E^* + \Delta E) - N(E^*)|$ versus $\ln |\Delta E|$ for $E^* = E_{\text{bot}} = -0.10373014133295410132683 \cdots$. The potential parameters correspond to those used in Fig. 1.

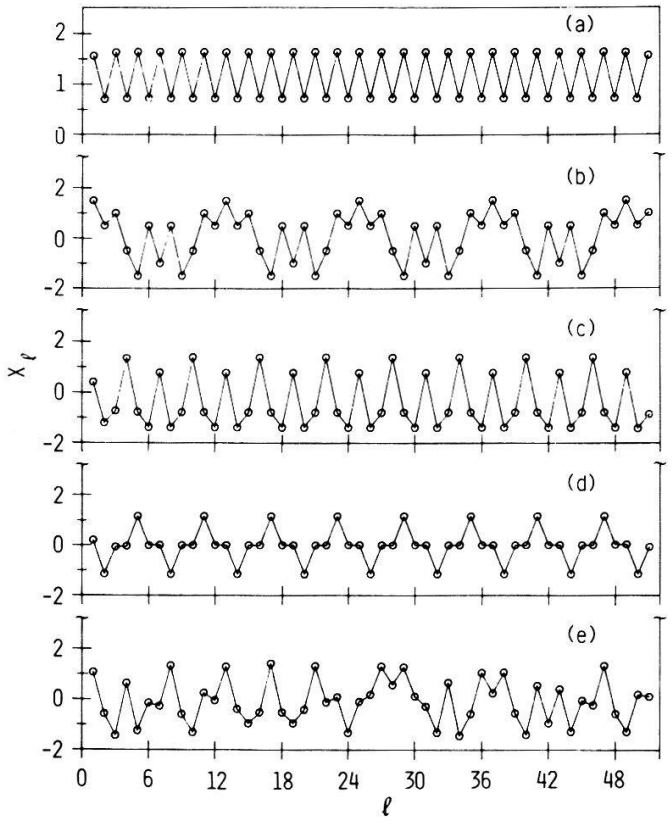

Figure 3
Trace map x_l versus length l for (a) ground-state two-cycle with $E = -0.10373014133295410132683 2\cdots$; (b) 12-cycle with $E = 0$; (c) six-cycle $(a, -b, -a, b, -a, -b)$ with $E = 2.2375398728152226936768\cdots$; (d) six-cycle $(0, 0, c, 0, 0, -c)$ with $E = 2.7822337314782, \ldots$, and (e) aperiodic solution with $E = 0.39558678454137556404259 79\cdots$. The potential parameters correspond to those used in Fig. 1.

yielding for the period of the scaling function $\Delta p \sim 2.119\cdots$ and for the slope $\bar{x} \sim 0.4541\cdots$. These estimates agree very well with the scaling behavior shown in Fig. 2.

Another interesting feature appears at *zero energy* for potential values $W_A = -W_B = 1$ where $N(E^* = 0) = 1/\sigma_G^4$. At this point, the trace map leads to a 12-cycle $(\frac{3}{2}, \frac{1}{2}, 1, -\frac{1}{2}, -\frac{3}{2}, \frac{1}{2}, -1, \frac{1}{2}, -\frac{3}{2}, -\frac{1}{2}, 1, \frac{1}{2})$ starting exactly with $\frac{3}{2}$ and without any pre-image. This 12-cycle is depicted in Fig. 3b.

We have also found the *six-cycles* $(a, -b, -a, b, -a, -b)$ and $(0, 0, c, 0, 0, -c)$ as well as *aperiodic solutions* which are well-known from the tight-binding model. The amplitudes a, b of the six-cycle $(a, -b, -a, b, -a, -b)$ lead to the first-mentioned six-cycle following from expressions (19), and are identical to those of the two-cycle. The scaling exponent $\bar{x}$ of the integrated density of states, $\bar{x} = 6 \ln \sigma_G / |\ln |\lambda||$, and the period of the scaling function $\Delta p = |\ln |\lambda||$ are then obtained from the trace map (15) by linearization around the six-cycle $(a, -b, -a, b, -a, -b)$. Linearization around the other six-cycle, $(0, 0, c, 0, 0, -c)$, leads to the three eigenvalues 1, λ and $1/\lambda$, where $\lambda = 8c^4 + 1 + 4c^2\sqrt{4c^4 + 1}$. The value of c can be evaluated from $c^2 = I - 1$, where the invariant I is given by equation (18). The six-cycle $(a, -b, -a, b, -a, -b)$ is depicted in Fig. 3c, while Fig. 3d shows the $(0, 0, c, 0, 0, -c)$ cycle, and Fig. 3d illustrates the aperiodic behavior.

Next, we turn to the derivation of the transmission coefficient in terms of the scalar recursion relation (13). Considering

$$\mathbf{P}_N = \prod_{n=N}^{1} \mathbf{P}^n = (\mathbf{T}^{N+1})^{-1} \prod_{n=N}^{1} \{\mathbf{T}^{n+1}\mathbf{P}^n(\mathbf{T}^n)^{-1}\}\mathbf{T}^1 = (\mathbf{T}^{N+1})^{-1}\tilde{\mathbf{P}}_N\mathbf{T}^1, \tag{26}$$

we find that the matrix element P_N^{11} is related to $\tilde{P}_N^{11}$ through

$$P_N^{11} = \frac{\{(e^{ik\Delta_1}\tilde{P}_N^{11} + \tilde{P}_N^{12}) - e^{-ik\Delta_{N+1}}(e^{ik\Delta_1}\tilde{P}_N^{21} + \tilde{P}_N^{22})\}}{e^{ik\Delta_{N+1}} - e^{-ik\Delta_{N+1}}}. \tag{27}$$

Now if we introduce the following initial condition for amplitudes $(\phi_1, \phi_0) = (e^{ik\Delta}1, 1)$, the expression for the matrix element P_N^{11} can be rewritten in the form $P_N^{11} = (\phi_{N+1} - e^{ik\Delta_{N+1}}\phi_N)/2i \sin(k\Delta_{N+1})$ leading to the following simple expression for the transmission [18]:

$$\tau_N = \frac{1}{|P_N^{11}|^2} = \frac{4\,|\sin(k\Delta_{N+1})|^2}{|\phi_{N+1} - e^{-ik\Delta_{N+1}}\phi_N|^2}. \tag{28}$$

Thus, evaluation of the energy dependence of the transmission for a chain of length N, has been reduced to evaluation of the amplitudes (ϕ_N, ϕ_{N-1}) from the scalar recursion relation (13).

As an example, we consider the transmission coefficient τ_N at energy $E = 2.2375398728152226936768\cdots$. The N-dependence on the real lattice is depicted in Fig. 4. Superimposed to an average slope, corresponding to decreasing transmission, there is a periodic structure $S_{F_l} = S_{F_{l+2}}$ owing to the six-cycle $(a, -b, -a, b, -a, -b)$ occurring in the trace map at this energy (Fig.

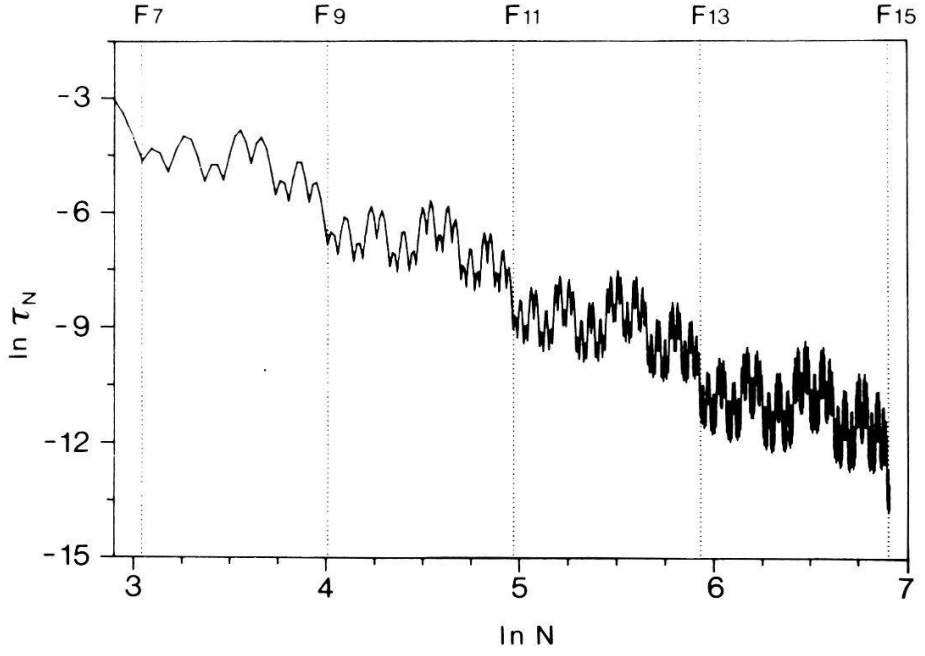

Figure 4
Transmission $\ln \tau_N$ versus real system length $\ln N$ for $E = 2.2375\cdots$ where the trace map exhibits the six-cycle $(a, -b, -a, b, -a, -b)$. Vertical bars mark the Fibonacci sites F_l. The potential parameters correspond to those used in Fig. 1.

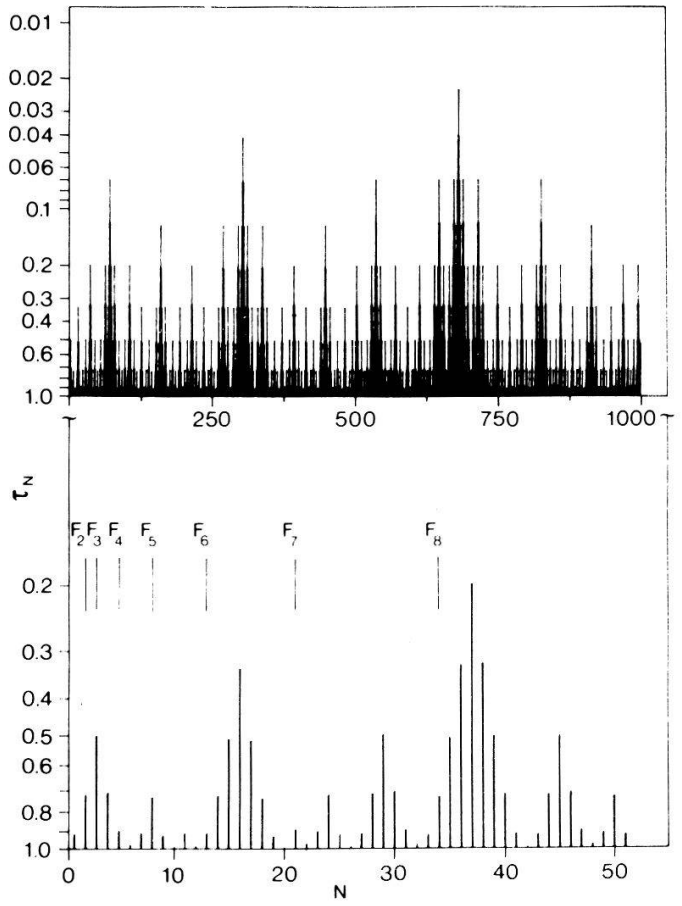

Figure 5
Transmission τ_N versus real system length N for $E = 2.7822\cdots$ where the trace map exhibits the six-cycle $(0, 0, c, 0, 0, -c)$. Note the negative logarithmic scale.

3c). The period two seen in the transmission is not in disagreement with the six-cycle, because the transmission is insensitive to the sign of a and b [equation (9)]. On the real lattice, however, the periodic structure appearing on the Fibonacci sublattice, is seen to give rise to self-similar behavior. A more quantitative exposition of the self-similar peak structure in τ_N is depicted in Fig. 5 for the six-cycle $(0, 0, c, 0, 0, -c)$ occurring at $E = 2.7822337314782\cdots$. Here, transmission τ_N is seen to be periodic on the Fibonacci sublattice, $\tau_{F_l} = \tau_{F_{l+3}}$. In analogy to the tight-binding model discussed in [6] and [19], in the transmission we observe series of peaks decreasing algebraically on a given sublattice, e.g. on the sublattice $F_3 + \cdots + F_{3\times 2p}$ or $1 + F_2 + \cdots + F_{3\times(2p+1)}$. The self-similarity of the peak structure can then be described by a scale transformation, yielding the scaling law $\tau_N \sim N^{-\beta}$, with the scaling exponent β. Furthermore, on the Fibonacci sublattice, F_l transmission τ_{F_l} has periodicity six and hence $\beta = 0$. Recognizing that there are many other sequences, as in th tight-binding model, we expect a distribution of β-values [6]. Comparing the lower and upper parts of Fig. 5, the self-similar structure is clearly seen. Next, we explore the implications of self-similarity in the energy window $E = 2.7822\cdots \pm 0.48$, where E corresponds to the value where the trace map exhibits the six-cycle $(0, 0, c, 0, 0, -c)$. For this

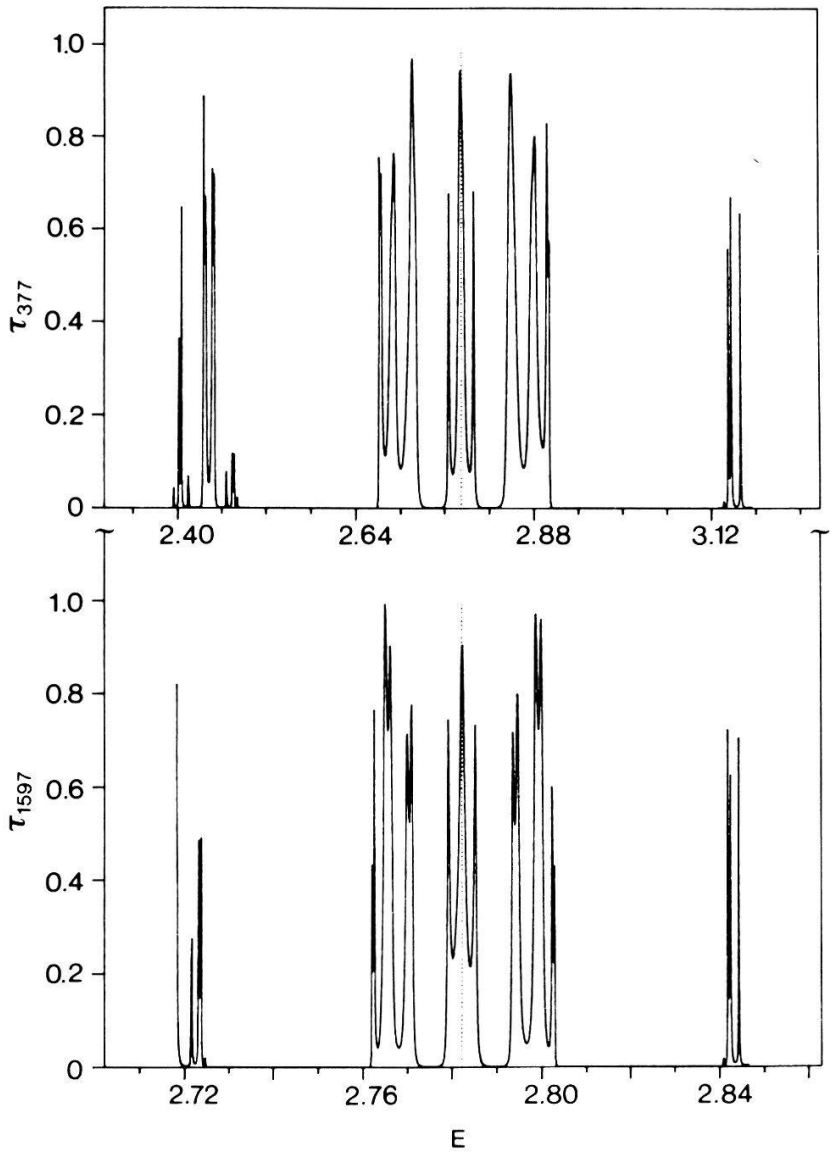

Figure 6
Transmission τ_N versus energy E around $E = 2.7822\cdots$ where the trace map exhibits the six-cycle $(0, 0, c, 0, 0, -c)$. $N = F_{13} = 377$ in the upper part and $N = F_{16} = 1597$ in the lower part. The dotted vertical line marks $E = 2.7822\cdots$.

purpose, we calculated the energy dependence of τ_N for $N = F_{13} = 377$ and $N = F_{16} = 1597$. The results are shown in Fig. 6 and exhibit striking self-similarities. The resulting scaling behavior can be understood in analogy to that of the integrated density of states [equation (24)]. Thus, $\tau_N(E^* - \Delta E)$ versus $\ln|E^* - \Delta E|$ is a periodic function with period $\Delta p = |\ln|\lambda|_{\max}|$.

3. Rectangular potential barriers

In this section, we extend our study to a rectangular array of barriers. Such a model represents a first step towards a realistic description of real superlattices.

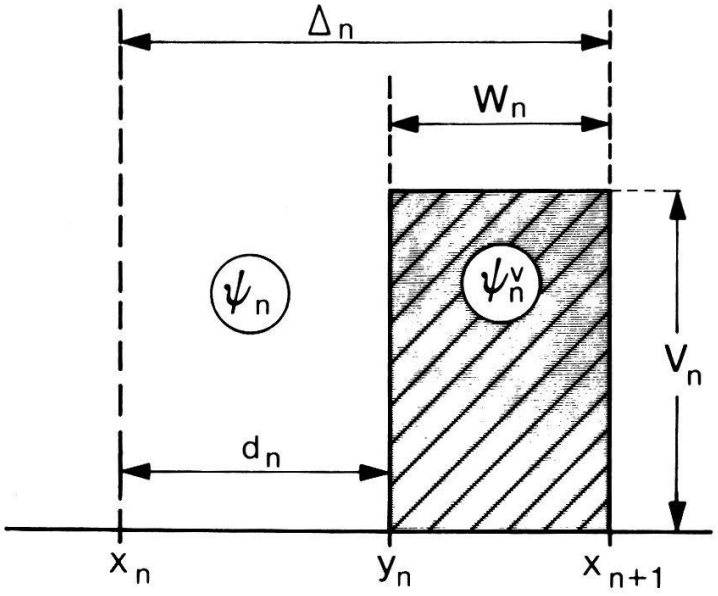

Figure 7
Unit cell used to build the Fibonacci superlattice.

The Schrödinger equation then reads

$$-\frac{\hbar^2}{2m}\frac{\partial^2\psi(x)}{\partial x^2}+V(x)\psi(x)=E\psi(x). \tag{29}$$

The potential $V(x)$ is constructed from two different elements A and B. The elements consist of a region of zero potential followed by a region with a rectangular barrier of width $w_{A,B}$ and height $V_{A,B}$. The lattice constants for the two elements are denoted by $\Delta_{A,B}$.

We can now follow the procedures outlined in the previous section to derive matrix and scalar recursion relations for the amplitudes of the wavefunctions, the trace map and the transmission coefficent. The n-th cell of the Fibonacci lattice is shown in Fig. 7. In the two subintervals $[x_n, y_n]$ and $[y_n, x_{n+1}]$ the Schrödinger equation (29) has the solutions:

$$\begin{aligned}\psi_n(x)&=A_n e^{ik(x-x_n)}+B_n e^{-ik(x-x_n)}, \qquad x_n<x<y_n,\\ \psi_n^v(x)&=A_n^v e^{i\kappa_n(x-y_n)}+B_n^v e^{-i\kappa_n(x-y_n)}, \qquad y_n<x<x_{n+1},\end{aligned} \tag{30}$$

where wavenumbers k and κ_n are given by the formulas $k=\sqrt{E}$ and $\kappa_n=\sqrt{E-V_n}$, respectively. Matching the wavefunctions, for the elements P_{ij}^n of the unimodular transfer matrix $\mathbf{P}^n$ we find

$$\begin{aligned}P_{11}^n&=\left\{\cos(\kappa_n w_n)-i\frac{\eta_n^+}{2}\sin(\kappa_n w_n)\right\}e^{ikd_n}, \qquad P_{12}^n=-i\frac{\eta_n^-}{2}\sin(\kappa_n w_n)e^{-ikd_n},\\ P_{21}^n&=i\frac{\eta_n^-}{2}\sin(\kappa_n w_n)e^{ikd_n}, \qquad P_{22}^n=\left\{\cos(\kappa_n w_n)+i\frac{\eta_n^+}{2}\sin(\kappa_n w_n)\right\}e^{-ikd_n},\end{aligned} \tag{31}$$

where $d_n=y_n-x_n$ is the distance between the potential barriers, $w_n=x_{n+1}-y_n$ the width of the barriers and $\Delta_n=d_n+w_n$ the length of the n-th cell, as shown in

Fig. 7, and $\eta^{\pm}$ is given by $\eta^{\pm} = -(\kappa_n/k \pm k/\kappa_n)$. Note that we have assumed no change in the effective mass when going from one region with zero potential into a barrier with $V(x) \neq 0$.

A real scalar recursion relation $\phi_{n+1} = \tilde{P}^n_{11}\phi_n + \tilde{P}^n_{12}\phi_{n-1}$ is again obtained by a transformation of the amplitudes of the wavefunctions $(\phi_{n+1}, \phi_n) = T^{n+1}(A_n, B_n)$, where the transformation matrix T^n has matrix elements $T^n_{11} = P^n_{11} + P^n_{21}$, $T^n_{12} = P^n_{12} + P^n_{22}$ and $T^n_{21} = T^n_{22} = 1$. The matrix elements of the promotion matrix $\tilde{P}^{n,n+1}_{ij}$ connecting the amplitudes ϕ_n of adjacent sites $(\phi_{n+1}, \phi_n) = \tilde{\mathbf{P}}^{n,n+1}(\phi_n, \phi_{n-1})$ are then given by

$$\tilde{P}^{n,n+1}_{11} = -\frac{\det T^{n+1}}{\det T^n}(P^n_{12} + P^n_{21}) + \frac{T^n_{12}T^{n+1}_{12} - T^n_{21}T^{n+1}_{21}}{\det T^n},$$
$$\tilde{P}^{n,n+1}_{12} = -\frac{\det T^{n+1}}{\det T^n}, \tag{32}$$

and $\tilde{P}^{n,n+1}_{21} = 1$, $\tilde{P}^{n,n+1}_{22} = 0$, leading to a fictitious tight-binding problem with additional non-constant off-diagonal matrix elements. Note that the whole matrix $\tilde{\mathbf{P}}^{n,n+1}$ has real elements, which can be expressed in the form of trigonometric and hyperbolic functions.

The trace-map relation $x_{l+1} = 2x_l x_{l-1} - x_{l-2}$ with initial conditions

$$\begin{aligned} x_{-1} = &\left\{\cos(\kappa_A w_A)\cos(\kappa_B w_B) + \frac{\eta^+_A\eta^+_B - \eta^-_A\eta^-_B}{4}\sin(\kappa_A w_A)\sin(\kappa_B w_B)\right\} \\ &\times \cos(kd_A - kd_B) \\ &+ \tfrac{1}{2}\{\eta^+_A \sin(\kappa_A w_A)\cos(\kappa_B w_B) - \eta^+_B \sin(\kappa_B w_B)\cos(\kappa_A w_A)\} \\ &\times \sin(kd_A - kd_B) \\ x_0 = &\cos(\kappa_B w_B)\cos(k_B d_B) + \frac{\eta^+_B}{2}\sin(\kappa_B w_B)\sin(k_B d_B), \\ x_1 = &\cos(\kappa_A w_A)\cos(k_A d_A) + \frac{\eta^+_A}{2}\sin(\kappa_A w_A)\sin(k_A d_A), \end{aligned} \tag{33}$$

and invariant $I = x^2_{-1} + x^2_0 + x^2_1 - 2x_{-1}x_0x_1 - 1$ allows, as in the case of δ potentials, identification and characterization of the states. Since invariant I depends on wavenumber k or energy E, we again expect self-similar and multifractal behavior.

Finally, the transmission coefficient τ_N on the real lattice can be evaluated from the amplitudes (ϕ_{N+1}, ϕ_N) of the scalar recursion relation (13) and (32) with suitable initial conditions (ϕ_1, ϕ_0). However, by sitting on the Fibonacci sublattice it is numerically more convenient to multiply the transfer matrices $\mathbf{P}_{l+1} = \mathbf{P}_{l-1}\mathbf{P}_l$ and to evaluate the transmission directly via equation (9). Note that formulas (31)–(33) reduce in the limit $w_n \to 0$, $d_n \to \Delta_n$, $V_n w_n \to W_n$ and $\eta^{\pm}_n \to W_n/k$ to the results (5), (12) and (16), as derived for the δ-function potentials.

We have now obtained the recursion relations for all physical quantities of Fibonacci chains with rectangular potential barriers. Before turning to typical

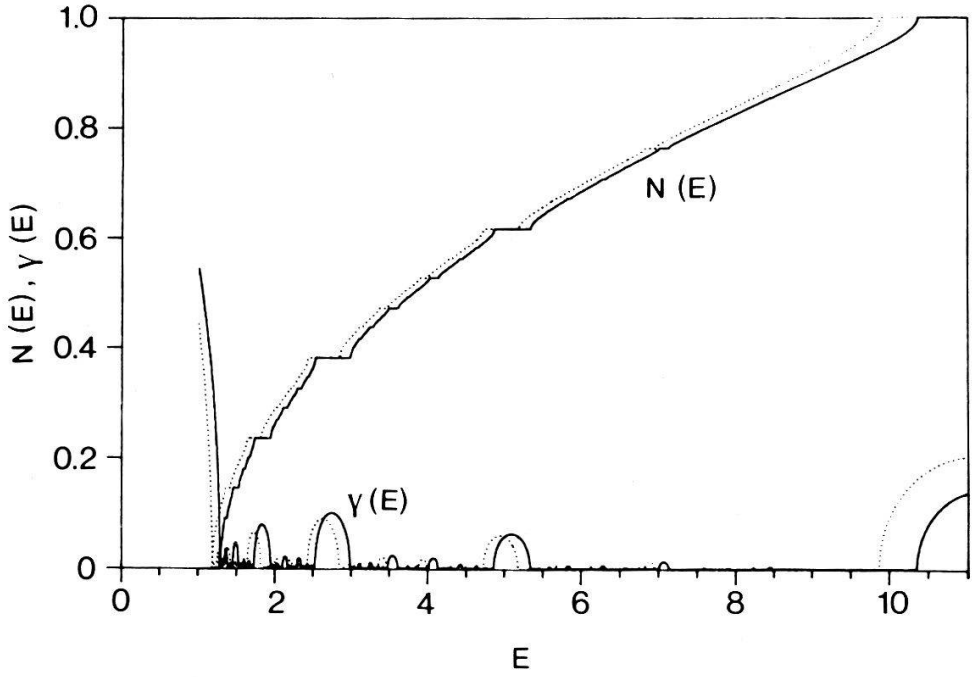

Figure 8
Integrated density of states $N(E)$ and inverse localization length $\gamma(E)$ versus energy for the rectangular barrier model (full curve). For comparison, we included $N(E)$ of the δ-function model (dotted curve). The parameters are: $V_A = -V_B = 2$, $w_A = w_B = \frac{1}{2}$, $\Delta_A = \Delta_B = 1$, and $W_A = -W_B = 2$, $N \sim 10^6$.

examples, we reconsider a periodic arrangement with periodic boundary conditions. The eigenvalues of a free particle are two-fold degenerate. Thus, a perturbation may lead to splitting. In the well-known periodic lattice, the eigenstates with wavenumbers $k = \pm p\pi$, $p = 1, 2, \ldots$, split and energy gaps are formed. Eigenstates with wavenumber different from $p\pi$ do not split. This means that the trace of the transfer matrix for a periodic lattice oscillates as a function of E between -2 and 2 in the regions of allowed energies. At energies where splitting occurs, the absolute value of the trace is larger than 2 and accordingly the forbidden energy levels can be determined from $|\frac{1}{2}\,\mathrm{Tr}\,\mathbf{P}| > 1$.

Similarly, forbidden energy levels appear in the spectrum of a Fibonacci superlattice with rectangular barriers. This is illustrated in Fig. 8. For comparison, we have included the δ-function potential limit. The parameters for the rectangular potential barriers with equal lattice spacings $\Delta_A = \Delta_B = 1$ are $V_A = V_B/2 = 2$, $w_A = w_B = \frac{1}{2}$ which yields $W_A = W_B/2 = 1$ in the δ-function limit. Although the potential barriers are very far from the δ-potential limit, both integrated density of states and inverse exponential localization length agree rather well and exhibit the same qualitative behavior.

Finally, we turn to the model with identical potential barriers $V_A = V_B = 2.5$ and $w_A = w_B = 0.4$, but with different lattice constants: $\Delta_A = 1/\sigma_G$ and $\Delta_B = \sigma_G$. The lattice constants are chosen in such a way that the mean lattice spacing ΔL equals unity. Figure 9 shows $N(E)$ for a lattice of size $F_{14} = 610$ in terms of a histogram, where each vertical bar marks the position of an eigenvalue. These results clearly reveal the formation of a fragmented integrated density of states in

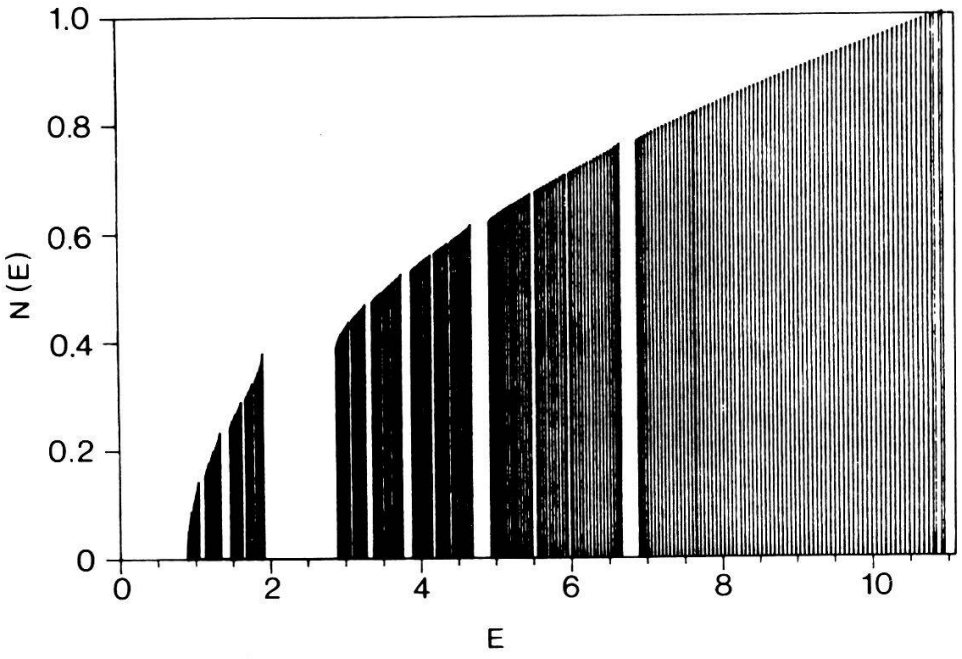

Figure 9
Histogram of the integrated density of states $N(E)$ versus energy E for the rectangular barrier model for a system of length $F_{14} = 610$. Each vertical bar marks the position of an energy eigenvalue. The potential parameters are $V_A = V_B = 2.5$, $w_A = w_B = 0.4$, $\Delta_A = 1/\Delta_B = 1/\sigma_G$.

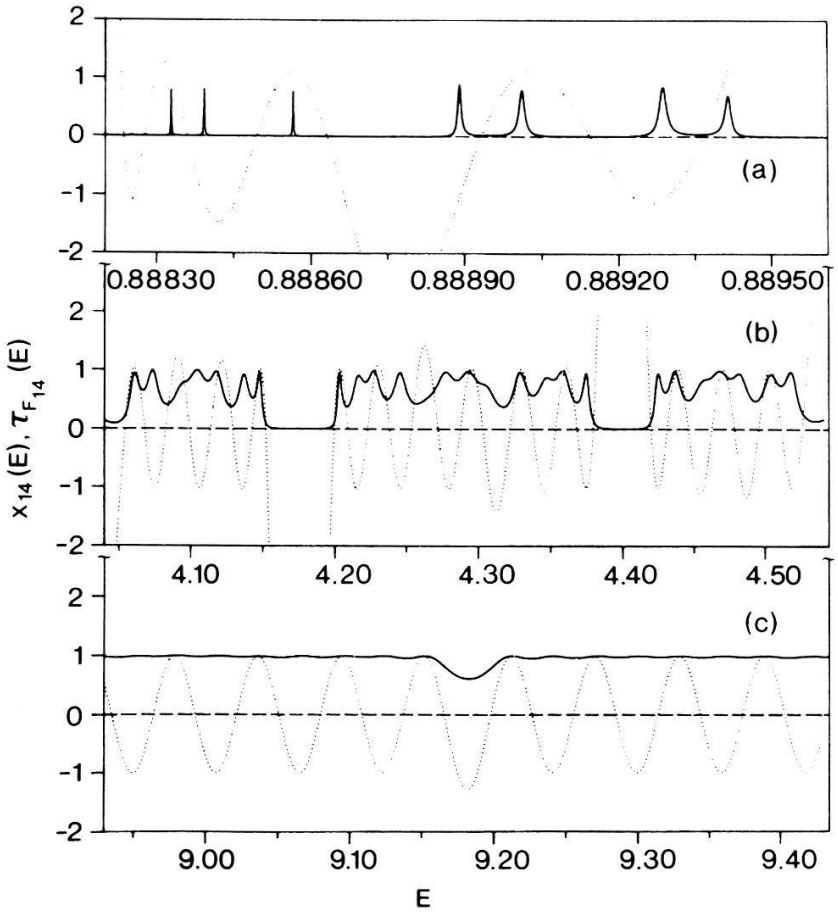

Figure 10
Energy dependence of x_{14} (dotted curve) and transmission $\tau_{F_{14}}$ (full curve) for three different typical energy regions: (a) near the ground state; (b) in the middle part, and (c) in the upper part of the spectrum. The other parameters correspond to those used in Fig. 9.

the infinite system, and strong fragmentation at low energies. To analyze some of their features and their implications for the trace and transmission, in Fig. 10 we show the energy dependence of these quantities in three different energy regions, namely at the bottom, middle and top of the spectrum for $F_{14} = 610$. Adopting periodic boundary conditions, the trace $x_{14}(E)$ depicted in Fig. 10a shows splitting of all states except for the ground state. The transmission coefficient indicates resonance tunneling at eigenenergies corresponding to both periodic ($x_{14} = 1$) and anti-periodic ($x_{14} = -1$) boundary conditions. Furthermore, τ_{14} only attains its maximum value at one of the two split energies and resonance tunneling does not occur at each split energy. Frequently, resonance tunneling occurs at energies which are slightly shifted from an exact energy eigenvalue. In cases where the splitting is weak, τ_{14} can attain its maximum between two split energies. This is peculiar as it corresponds to tunneling in a forbidden gap, but in cases of strong splitting where we have a clearly formed energy gap this does not happen. As the energy increases, τ_{14} becomes broader as seen in Fig. 10b. In the forbidden gaps, τ_{14} decreases rapidly to zero. At the gap edges, the transmission coefficient is less broad which is consistent with the fact that electrons with energies close to a band edge are algebraically localized. Finally, Fig. 10c shows x_{14} and τ_{14} for energy values in the upper part of the spectrum. We observe band-like behavior where the transmission coefficient approaches one.

4. Conclusions

Two different models have been considered to investigate the spectrum and the transmission properties of the Krönig–Penney model on a Fibonacci superlattice. Specifically, we have treated the δ-function type model and a potential barrier model. The latter is expected to mimic real Fibonacci superlattices which can be fabricated by molecular-beam epitaxy. Using the transfer-matrix technique, we have reduced the continuous Schrödinger problem to an associated tight-binding version, allowing further transformation to a real and scalar recursion relation. Thus, matrix multiplications are eliminated and both integrated density of states and exponential growth rate are simply determined by iterating the scalar map. Moreover, the transmission coefficient, determining the resistance, also follows from the recursion relation. Scaling properties of the spectrum have been derived from the fixed-point analysis of the two-, six- and 12-cycles in the trace map. The ground state leads to a two-cycle, while at gap edges, six- and 12-cycles appear. We also found internal energies, surrounded by cycles, where the trace map exhibits aperiodic behavior under iterations. Finally, band-like behavior was found at sufficiently high energies, where the barriers become irrelevant. In contrast to the periodic case, the integrated density of states is very fragmented for low energies, where the invariant of the trace map is large. In this region, the system has an infinite number of gaps and energies belonging to the spectrum having measure zero. Nevertheless, there are many special energies which belong to the spectrum. At high energies, however, the

situation is just the opposite. Apparently, the size of the gaps tends to zero, so that asymptotically almost all the energies belong to the spectrum. Our results for the transmission revealed interesting self-similar behavior. This feature is absent in periodic and random superlattices, and suggests interesting applications.

Acknowledgment

We should like to thank Drs. P. Guéret and W. Schlup for valuable discussions. Two of the authors (TS and MPS) gratefully acknowledge financial support from the Danish Technical Research Council and from IBM Denmark.

REFERENCES

[1] R. KRÖNIG and W. G. PENNEY, Proc. R. Soc. London *130*, 499 (1931).
[2] P. LEE and T. V. RAMAKRISHNAN, Rev. Mod. Phys. 57, *287* (1985), and references therein.
[3] F. J. WEGNER, Z. Phys. B*25*, 327 (1976); E. ABRAHAMS, P. W. ANDERSON, D. C. LICIARDELLO and T. V. RAMAKRISHNAN, Phys. Rev. Lett. *42*, 673 (1979).
[4] J. B. SOKOLOFF, J. Phys. C*17*, 1703 (1984), and references therein.
[5] B. SIMON, Adv. Appl. Math. *3*, 463 (1982), and references therein.
[6] T. SCHNEIDER, A. POLITI and D. WÜRTZ, Z. Phys. B*66*, 469 (1987).
[7] M. KOHMOTO, L. P. KADANOFF and C. TANG, Phys. Rev. Lett. *50*, 1870 (1983); S. OSTLUND, R. PANDIT, D. RAND, H. J. SCHELLNHUBER and E. SIGGIA, Phys. Rev. Lett. *50*, 1873 (1983).
[8] E. H. C. PARKER, *The Technology and Physics of Molecular Beam Epitaxy* (Plenum, N.Y. 1983).
[9] See, e.g., E. MERZBACHER, *Quantum Mechanics* (Wiley, N.Y. 1961).
[10] H. SCHMIDT, Phys. Rev. *105*, 425 (1957).
[11] T. M. NIEWENHUIZEN, Physica *120A*, 468 (1983).
[12] P. ERDÖS and R. C. HERNDON, Adv. Phys. *31*, 65 (1982).
[13] J. KOLLAR and A. SÜTO, Phys. Lett. A*117*, 203 (1986).
[14] P. HU and C. S. TING, Phys. Rev. B*34*, 8331 (1986).
[15] J. BELLISARD, A. FORMOSO, R. LIMA and D. TESTARD, Phys. Rev. *B26,* 3024 (1982).
[16] T. SCHNEIDER, in *Lecture Notes in Physics 268,* L. Garrido, Ed. (Springer, Berlin 1987) p. 199.
[17] J. M. LUCK and T. M. NIEWENHUIZEN, Europhys. Lett. *2*, 257 (1986).
[18] C. M. SOUKOULIS, J. V. JOSÉ, E. N. ECONOMOU and P. SHENG, Phys. Rev. Lett. *50*, 764 (1983).
[19] M. KOHMOTO and J. R. BANAVAR, Phys. Rev. B*34*, 563 (1986).